

## MASS FUNCTION OF LOW MASS DARK HALOS

HIDEKI YAHAGI<sup>1</sup>

Division of Theoretical Astrophysics, National Astronomical Observatory of Japan, Tokyo 181-8588, Japan

MASAHIRO NAGASHIMA

Department of Physics, University of Durham, South Road, Durham DH1 3LE, U. K.

AND

YUZURU YOSHII<sup>2</sup>

Institute of Astronomy, University of Tokyo, 2-21-1 Osawa, Mitaka, Tokyo 181-0015, Japan

## ABSTRACT

The mass function of dark halos in a  $\Lambda$ -dominated cold dark matter ( $\Lambda$ CDM) universe is investigated. 529 output files from five runs of  $N$ -body simulations are analyzed using the friends-of-friends cluster finding algorithm. All the runs use  $512^3$  particles in the box size of  $35 h^{-1}\text{Mpc}$  to  $140 h^{-1}\text{Mpc}$ . Mass of particles for  $35 h^{-1}\text{Mpc}$  runs is  $2.67 \times 10^8 h^{-1} M_\odot$ . Because of the high mass resolution of our simulations, the multiplicity function in the low-mass range, where the mass is well below the characteristic mass and  $\bar{\delta} = \bar{\delta}_c = 1.0$ , is evaluated in the present work, and is well fitted by the functional form proposed by Sheth & Tormen (ST). However, the maximum value of the multiplicity function from our simulations at  $\bar{\delta} = 1$  is smaller, and its low mass tail is shallower when compared with the ST multiplicity function.

*Subject headings:* cosmology: theory — dark matter — galaxies: luminosity function, mass function

## 1. INTRODUCTION

The mass function is one of the most important statistical quantities of dark halos. Press & Schechter (1974) invented an ansatz to predict the mass function of dark halos formed through hierarchical clustering, assuming that each smoothed mass element with arbitrary smoothing length evolves independently, in accordance with the spherical top-hat model. The PS formalism was extended so that the merging history of each halo is traceable (Bond et al. 1991; Bower 1991; Lacey & Cole 1993). This extended PS formalism has been used in a wide range of applications. Especially the so-called semi-analytic galaxy models (Cole et al. 2000; Kauffmann, White, & Guiderdoni 1993; Nagashima et al. 2001; Somerville & Primack 1999) use it to successfully reproduce many properties of observed galaxies.

The PS mass function and the mass function from  $N$ -body simulations agree with each other only qualitatively (Brainerd & Villumsen 1992; Efstathiou et al. 1988), and modification to threshold linear overdensity leads to a better agreement (Efstathiou & Rees 1988; Gelb & Bertschinger 1994; Lacey & Cole 1994). However, the PS mass function gives the smaller number of high-mass halos (Gross et al. 1998; Jain & Bertschinger 1994), while giving the larger number of low-mass halos when compared with the  $N$ -body mass functions (Governato et al. 1999; Somerville et al. 2000). This tendency was confirmed over a mass range by connecting the numerical mass functions from simulations with different box sizes (Gross et al. 1998; Jenkins et al. 2001). Taking into account the spatial correlation of density fluctuations (Nagashima 2001; Yano, Nagashima, & Gouda 1996), or incorporating the ellipsoidal collapse model into the PS ansatz instead of the spherical collapse model (Audit, Teyssier, &

Alimi 1997; Epstein 1984; Lee & Shandarin 1998; Monaco 1995; Sheth, Mo, & Tormen 2001; Sheth & Tormen 2002), an agreement was improved between the numerical mass function and the analytic mass function, especially the ST mass function proposed by Sheth & Tormen (1999). In addition, the mass function of cluster progenitors has also been studied (Okamoto & Habe 1999).

On the other hand, the numerical mass function depends on the cluster finding algorithm adopted (Gelb & Bertschinger 1994; Governato et al. 1999; Lacey & Cole 1993). Jenkins et al. (2001, hereafter J01) demonstrated that the friends-of-friends (FoF) algorithm (Davis et al. 1985) with a fixed linking length of 0.2 times the mean particle separation results in the numerical mass function that shows the best universality for various compositions of cosmological parameters and box sizes. Thus, it is better to set the threshold density proportional to the *background* mass density rather than to the *critical* density. White (2002, hereafter W02) supported the above argument and demonstrated that an other definition of mass of halos,  $M_{180b}$ , gives the universal numerical mass function. Here,  $M_{180b}$  is the mass within a sphere whose average density is 180 times the *background* density.

However, different authors support different mass functions. For example, J01 proposed a new fitting formula to the universal mass function, while W02 supported the ST mass function (see also Reed et al. 2003). Since the mass function of high-mass halos has extensively been studied by them, this discrepancy is possibly due to the lack of information on the behavior of the numerical mass function for low-mass halos. Thus, in order to investigate the functional form of the universal mass function, we performed five runs of  $N$ -body simulations with high mass resolution.

In this paper, we briefly describe our simulation code and cosmological and simulation parameters adopted in §2. Results of the simulations as well as the parameter values for the best-fit mass function are given in §3, and discussions are given in §4.

Electronic address: hideki.yahagi@nao.ac.jp

Electronic address: masahiro.nagashima@durham.ac.uk

<sup>1</sup> NAOJ Science Research Fellow<sup>2</sup> Research Center for the Early Universe, University of Tokyo, 7-3-1 Hongo, Bunkyo-ku, Tokyo 113-0033, Japan

## 2. MULTIPLICITY FUNCTION

The multiplicity function is the differential distribution function of the normalized fluctuation amplitude of dark halos for each mass element. According to the definition by Sheth & Tormen (1999), the multiplicity function is defined as

$$f(\delta) = M^2 \frac{n(M; z)}{d \log M}; \quad (1)$$

where  $n(M; z)$  is the number density of dark halos,  $\delta_c$  is the peak height of a halo,  $\delta_c$  is the linear overdensity at the collapse epoch of halos given by the spherical collapse model, and  $\sigma_M$  is the standard deviation of the density fluctuation field smoothed by the top-hat window function. Note that the time evolution of the number density and the dependence of the number density on the initial power spectrum are absorbed in  $\delta_c$ . Since this universality of the multiplicity function is guaranteed under the PS ansatz, we compare our simulation results with analytic multiplicity functions.

Along with the PS ansatz, Press & Schechter (1974) proposed the following analytic multiplicity function:

$$\text{PS: } f(\delta) = \frac{r}{2} \exp(-\delta^2/2); \quad (2)$$

This PS multiplicity function has successfully predicted the numerical multiplicity function in a qualitative manner. However, Sheth & Tormen (1999) proposed an alternative analytic multiplicity function that could better reproduce the numerical multiplicity function:

$$\text{ST: } f(\delta) = A(1 + \delta^{2p})^{-\frac{r}{2}} \exp(-\delta^2/2); \quad (3)$$

where  $\delta_c^2 = a^2$ , and  $A$  is a normalization factor defined so that  $\int_0^\infty f(\delta) d\delta = 1$ . Because of this unity constraint,  $A$  is not an independent parameter, but is expressed in forms of  $p$ :

$$A = \frac{1}{1 + 2^{-p} - 1/2} (1/2 - p)^{-1}; \quad (4)$$

Sheth & Tormen (1999) gave the best-fit parameter values of  $a = 0.707$ ;  $p = 0.3$ ; and  $A = 0.322$ . The PS multiplicity function is included in this ST multiplicity function with  $a = 1$ ;  $p = 0$ , and  $A = 1/2$ .

The ST multiplicity function has a maximum at  $\delta = \max$  that satisfies the following equation:

$$(\delta_c^{2p+1})(\delta_c^{2p} - 1) + 2p = 0; \quad (5)$$

where  $\delta_c^{2p} = a^{2p}$ . It is trivial to see  $\delta_c = 1$  for the case of the PS multiplicity function.

J01 also proposed an analytic multiplicity function which gives a fit to their numerical multiplicity function:

$$\text{J01: } f(\delta) = 0.315 \exp(-0.61 + \log \delta - \log \delta^2); \quad (6)$$

The valid range of this fitting formula is  $-1.2 < \log \delta - \log \delta_c < 1.05$ . Hereafter we assume that  $\delta_c$  in the above equation is constant and takes the value in the Einstein-de Sitter universe, i.e.  $\delta_c = (3/20)(12)^{2/3} = 1.686$  in order to compare the J01 multiplicity function with other functions.

## 3. SIMULATIONS AND RESULTS

We used the Adaptive Mesh Refinement  $N$ -body code developed by Yahagi (2002), which is a vectorized and parallelized version of the code described in Yahagi & Yoshii (2001). All five runs of simulations we performed adopt

the  $\Lambda$ CDM cosmological parameters of  $\Omega_m = 0.3$ ,  $\Omega_\Lambda = 0.7$ ,  $h = 0.7$ , and  $\sigma_8 = 1.0$ , using  $512^3$  particles in common. The size of the finest mesh is  $1/64$  of the base mesh, and the force dynamic range is  $2^{15} = 32768$ . Other simulation parameters, such as the box size and the particle mass are given in Table 1. Initial conditions were generated by the GRAFIC2 code provided by Bertschinger (2001) using the power spectrum given by Bardeen et al. (1986). Five runs produced 529 files, and each of them was analyzed by the FoF algorithm with a constant linking length of 0.2 times the mean particle separation. Details of the simulations will be given in Yahagi et al., in preparation.

The mass functions of dark halos are shown in Figure 1. The upper and lower panels show the mass functions at  $z = 3$  and  $z = 0$ , respectively. The PS mass function is represented by solid lines, and the ST mass function by dashed lines. At both redshifts, the numerical mass functions from our simulations agree with the ST mass function in a mass range of  $10^{10} M_\odot \sim M_\odot \sim 10^{13} M_\odot$ .

The numerical multiplicity functions are shown by crosses in five panels of Figure 2. All the data from the initial redshift to the present  $z = 0$  is compiled to draw the average curves (crosses) with error bars indicating the epoch to epoch variation. In the panel (f), all the numerical multiplicity functions are shown by thin lines. Dark halos that consist of less than 600 particles are not used in calculating the multiplicity function, and  $1/64$  dex-sized bins containing less than 100 halos are excluded to avoid the contamination of the rare objects. Three analytic multiplicity functions described in the previous section are also shown in this figure, that is PS (solid lines), ST (dashed lines), and J01 (dotted lines). The best-fit functions based on the ST functional form are also shown by dot-dashed lines. The best-fit parameters are given in Table 2 and are very close to those of W02. Since the data are available only in the region at  $\delta > 3$ , these functions could be erroneous at  $\delta < 3$ .

In most cases, the numerical multiplicity functions and the best-fit functions to them are consistent with the ST and J01 multiplicity functions at  $\delta > 3$ . However, each of the numerical multiplicity functions reside between the ST and J01 functions at  $1.5 < \delta < 3$ , and is below the ST function at  $\delta < 1$  except for the 35b run. The numerical multiplicity functions have an apparent peak at  $\delta = 1$ , instead of a plateau as seen in the J01 function. We here proposed the following function to fit to the numerical multiplicity function:

$$f(\delta) = A[1 + (B \delta^2)^C]^{-D} \exp[-(B \delta^2)^2]; \quad (7)$$

where,  $A$  is a normalization factor to satisfy the unity constraint,  $\int_0^\infty f(\delta) d\delta = 1$ , therefore

$$A = 2(B \delta^2)^D \int_0^\infty [D \delta^2 + (C + D) \delta^2] g^{-1}; \quad (8)$$

The best-fit parameters are given as  $B = 0.893$ ,  $C = 1.39$ , and  $D = 0.408$ , and from these parameters,  $A$  is constrained so that  $A = 0.298$ . This best-fit function from equation 7 is shown in Figure 3 and is only valid at  $0.3 < \delta < 3$ .

Since the unity constraint is only an assumption, we can relax this constraint and treat  $A$  as a free parameter. Actually, almost a half of the particles are not bound to any halos as shown in Table 3. On the other hand, the best-fit parameters without the unity constraint using equation 3 are  $A = 0.320$ ,  $B = 0.664$ ,  $C = 1.99$ , and  $D = 0.36$ , for which  $\int_0^\infty f(\delta) d\delta = 1.2713$ . Since the fraction of bound particle should not exceed unity, we assign the unity constraint to all the best-fit functions below.

We also investigate the peak position of the multiplicity functions. Since deriving  $\bar{m}_{\text{max}}$  directly from the numerical multiplicity function is difficult due to the numerical fluctuation around the maximum value, we derived  $\bar{m}_{\text{max}}$  from the best fit ST function by solving equation 5. These  $\bar{m}_{\text{max}}$  are given in Table 2, and are very close to unity. For reference,  $\bar{m}_{\text{max}} = 0.916$  for the J01 multiplicity function, and  $\bar{m}_{\text{max}} = 0.881$  for the multiplicity function proposed by Lee & Shandarin (1998).

We also checked the time dependence of the multiplicity function. Figure 4 shows the multiplicity function from the 35a run, for four redshift ranges of  $0 < z < 1$  (*circles*),  $1 < z < 3$  (*squares*),  $3 < z < 6$  (*triangles*), and  $z > 6$  (*crosses*). At high redshifts, high- $\bar{m}$  halos in the exponential part of the best-fit ST function and equation 7 are probed. As redshift decreases, the probe window moves to the lower- $\bar{m}$  region.

Since there are no modes of density fluctuations whose wave length is larger than the box size on which the periodic boundary is placed. The numerical multiplicity function is conditional such that  $f(\bar{m}_{\text{box}} = 0)$ , where  $\bar{m}_{\text{box}}$  is the density contrast smoothed over a mass scale comparable to the box size. Since our box size is smaller than that of other groups, we have estimated this box-size effect comparing the unconditional PS multiplicity function using the sharp  $k$ -space filter with the conditional one (Bond et al. 1991; Bower 1991; Lacey & Cole 1993),

$$f_c = \frac{\bar{m}}{2} \frac{1 - \bar{m}_{\text{box}}}{(1 - \bar{m}_{\text{box}})^{3/2}} \exp \left( -\frac{(\bar{m} - \bar{m}_{\text{box}})^2}{2(1 - \bar{m}_{\text{box}})} \right); \quad (9)$$

where  $\bar{m} = \bar{m}_{\text{box}}$ . Setting  $\bar{m}_{\text{box}} = 0$ , this effect is found to be not so large at  $\bar{m} \approx 3$  for the box size of  $35h^{-1}\text{Mpc}$ , and it makes the universality of the multiplicity function even worse.

#### 4. DISCUSSION

We have performed five runs of  $N$ -body simulations with high mass resolution in order to study the behavior of the numerical multiplicity function in the low-mass range, or the low- $\bar{m}$  region. Throughout the peak range of,  $0.3 < \bar{m} < 3$ , the ST functional form provides a good fit to them with parameter values of  $a = 0.664$ ;  $p = 0.321$ , and  $A = 0.301$ . These values are very close to those of W02. Our numerical multiplicity functions have a peak at  $\bar{m} \approx 1$  as in the ST function, instead of a plateau in the J01 function.

However, some detailed discrepancies are seen between our numerical multiplicity functions and the ST and J01 analytic functions. First, in the low- $\bar{m}$  region of  $\bar{m} < 1$ , our numerical multiplicity functions systematically fall below the ST and the J01 functions, while they are consistent with that of W02. On the other hand, in the high- $\bar{m}$  region, where  $\bar{m}$  is significantly larger than unity, our numerical multiplicity functions take values between the ST and J01 functions. Although these differences are within 1  $\sigma$  error bars, they are possibly due to the different box sizes adopted. Sheth & Tormen (1999) used

the data from the GIF simulations (Kauffman et al. 1999) with the box size of  $144h^{-1}\text{Mpc}$  or less, and W02 mainly used the data from the box size of  $200h^{-1}\text{Mpc}$ . On the other hand, J01 used the  $3000h^{-1}\text{Mpc}$  simulation at maximum. We have taken into account the box-size effect using the conditional PS multiplicity function (equation 9) but this effect is found to be too small to resolve this problem. Introducing the estimation using the conditional multiplicity function based on the unconditional multiplicity function which fits the numerical multiplicity function well, such as the ST multiplicity function, would resolve this problem. However, such an improved estimation of the box-size effect might be weaker than the estimation based on the PS function, because the unconditional ST function at  $\bar{m} \approx 1$  has a broad peak that is below that of the PS function. The fact that our numerical multiplicity functions keep the universality supports this line of argument.

Thus, there are two discrepancies remained. One is the discrepancy between the numerical and analytical multiplicity functions. Although our newly proposed functional form (equation 7) provides a better fit when compared with the ST functional form (equation 3), we need an analytic function based on a theoretical background which fits the numerical multiplicity function even better. The other one is the discrepancy in the numerical multiplicity functions from various simulation runs. There are three strategies to resolve this discrepancy. The first is to run simulations having still higher mass dynamic range free from the box size effect. The second is to increase the number of realizations as W02 did, because there is a scatter from the runs using the same box size. The third is to run simulations whose box size is *smaller* than that of the present work, although it might sound contradictorily. From simulations with smaller box size, we will obtain the information on the conditional multiplicity function which coincides with the unconditional multiplicity function at  $\bar{m} \approx 1$ . Comparing the unconditional multiplicity function from simulations with a large box size and the conditional multiplicity function from those of a small box size will offer not only the clues to resolve the above mentioned discrepancies, but also insights into the mechanism how the PS ansatz works to reproduce the numerical multiplicity function.

Simulations described in this paper were carried out using Fujitsu-made vector parallel processors VPP5000 installed at the Astronomical Data Analysis Center, National Astronomical Observatory of Japan (ADAC/NAOJ), under the ADAC/NAOJ large scale simulation projects (group-ID: myy26a, yhy35b). HY would like to thank Joseph Silk and Masahiro Takada for their useful comments. MN acknowledges support from a PPARC rolling grant for extragalactic astronomy and cosmology. This work has been supported partly by the Center of Excellence Research (07CE2002) of the Ministry of Education, Science, Culture, and Sports of Japan.

#### REFERENCES

- Audit, E., Teyssier, R. & Alimi, J.-M. 1997, *A&A*, 325, 439  
 Bardeen, J. M., Bond, J. R., Kaiser, N., & Szalay, A. S. 1986, *ApJ*, 304, 15  
 Bertschinger, E. 2001, *ApJS*, 137, 1  
 Bond, J. R., Cole, S., Efstathiou, G., & Kaiser, N. 1991, *ApJ*, 379, 440  
 Bower, R. G. 1991 *MNRAS*, 248, 332  
 Brainerd, T. G., & Villumsen, J. V. 1992, *ApJ*, 394, 409  
 Cole, S., Lacey, C. G., Baugh, C. M., & Frenk, C. S. 2000, *MNRAS*, 319, 168  
 Davis, M., Efstathiou, G., Frenk, C. S., & White, S. D. M. 1985, *ApJ*, 292, 371  
 Efstathiou, G., Frenk, C. S., White, S. D. M., & Davis, M. 1988, *MNRAS*, 235, 715  
 Efstathiou, G., & Rees, M. J. 1988, *MNRAS*, 230, 5p  
 Epstein, R. I. 1984, *ApJ*, 281, 545  
 Gelb, J. M., & Bertschinger, E. 1994, *ApJ*, 436, 467  
 Governato, F., Babul, A., Quinn, T., Tozzi, P., Baugh, C. M., Katz, N., & Lake, G. 1999, *MNRAS*, 307, 949

- Gross, M. A. K., Somerville, R. S., Primack J. R., Holtzman, J., & Klypin, A. 1998, *MNRAS*, 301, 81
- Jain, B., & Bertschinger, E. 1994, *ApJ*, 431, 495
- Jenkins, A., Frenk, C. S., White, S. D. M., Colberg, J. M., Cole, S., Evrard, A. E., Couchman, H. M. P., & Yoshida, N. 2001, *MNRAS*, 321, 372
- Kauffmann, G., Colberg, J. M., Diaferio, A., & White, S. D. M. 1999, *MNRAS*, 303, 188
- Kauffmann, G., White, S. D. M., & Guiderdoni, B. 1993, *MNRAS*, 264, 201
- Lacey, C., & Cole, S. 1993, *MNRAS*, 262, 627
- Lacey, C., & Cole, S. 1994, *MNRAS*, 271, 676
- Lee, J., & Shandarin, S. F. 1998, *ApJ*, 500, 14
- Monaco, P. 1995, *ApJ*, 447, 23
- Nagashima, M. 2001, *ApJ*, 562, 7
- Nagashima, M., Totani, T., Gouda, N., & Yoshii, Y. 2001, *ApJ*, 557, 505
- Okamoto, T., & Habe, A. 1999, *ApJ*, 516, 591
- Press, W. H., & Schechter, P. 1974, *ApJ*, 187, 425
- Reed, D., Gardner, J., Quinn, T., Stadel, J., Fardal, M., and Lake, G. 2003, preprint (astro-ph/0301270)
- Sheth, R. K., Mo, H. J., & Tormen, G. 2001, *MNRAS*, 323, 1
- Sheth, R. K., & Tormen, G. 1999, *MNRAS*, 308, 119
- Sheth, R. K., & Tormen, G. 2002, *MNRAS*, 329, 61
- Somerville, R. S., Lemson, G., Kolatt, T. S., & Dekel, A. 2000, *MNRAS*, 316, 479
- Somerville, R. S., & Primack J. R. 1999, *MNRAS*, 310, 1087
- White, M. 2002, *ApJS*, 143, 241
- Yahagi, H. 2002, Doctoral Thesis, University of Tokyo
- Yahagi, H., & Yoshii, Y. 2001, *ApJ*, 558, 463
- Yano, T., Nagashima, M., & Gouda, N. 1996, *ApJ*, 466, 1

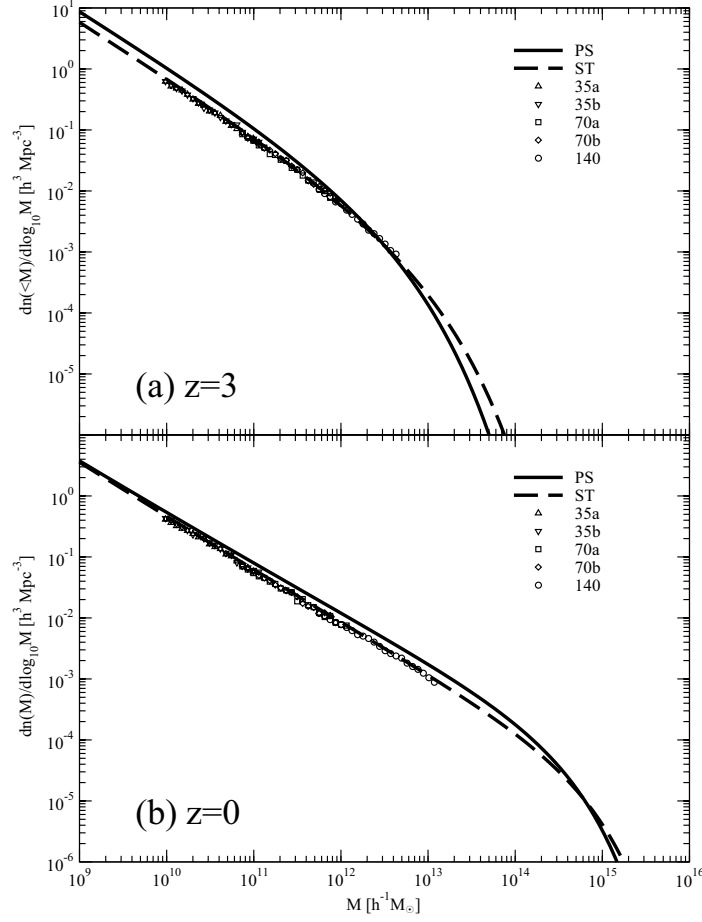


FIG. 1.— The mass functions of dark halos at (a)  $z=3$  and (b)  $z=0$ . The ST mass function (*dashed line*) agrees with the numerical mass functions (*symbols*) fairly well at both redshifts, while the PS mass function (*solid line*) does not agree with them.

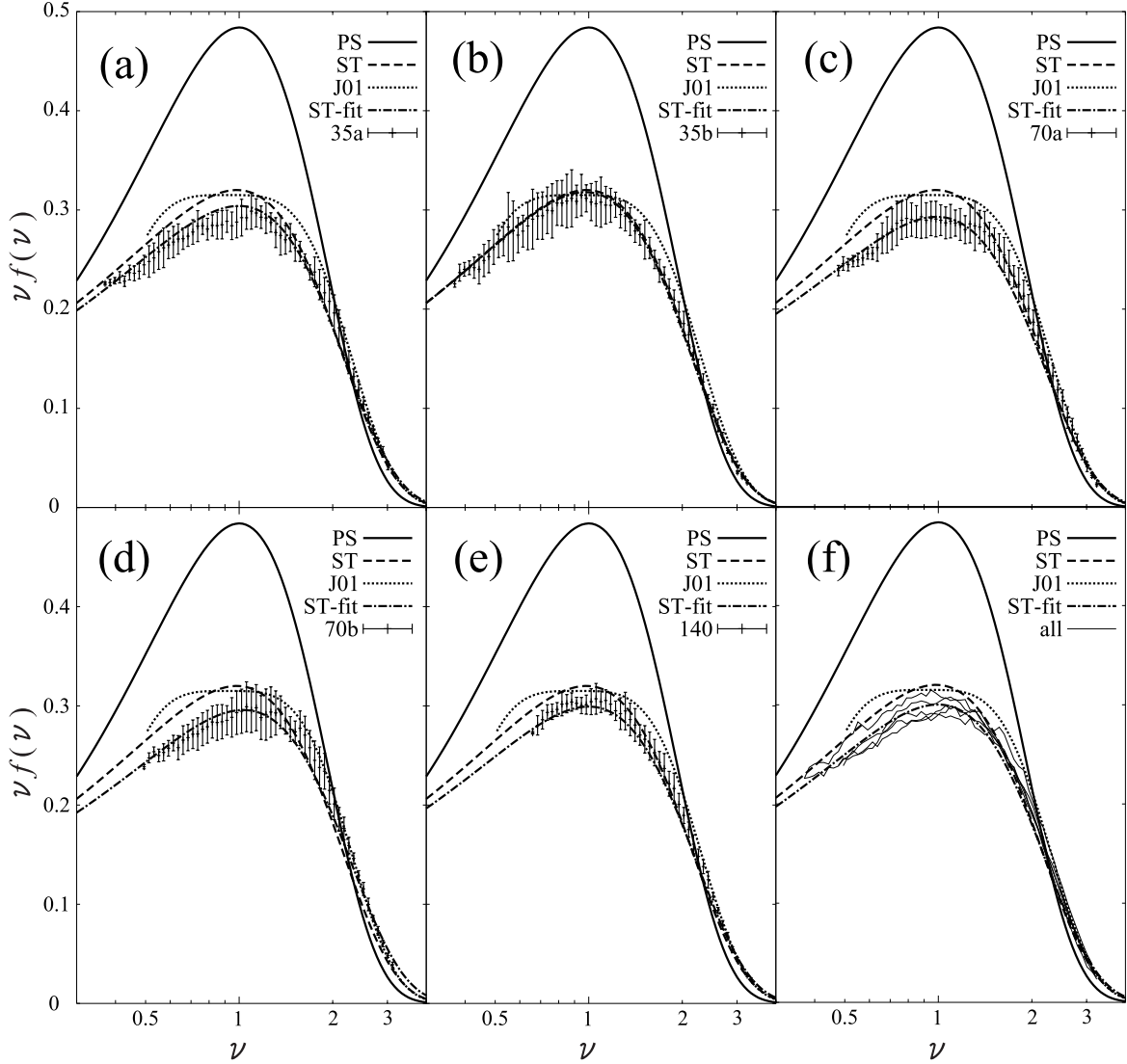


FIG. 2.— The numerical multiplicity functions from five runs of our simulations (*crosses with error bars*) are shown in the panels (a-e), except for the panel (f) which shows the results from all the runs (*thin lines*). The numerical multiplicity functions are derived by compiling all the data from the initial redshift to the present  $z=0$ . Crosses and error bars represent their average and rms, respectively. Also shown in each panel are the PS multiplicity function (*solid line*), the ST multiplicity function (*dashed line*), the J01 multiplicity function (*dotted line*), and the best-fit function using the ST functional form (*dot-dashed line*) for which adopted parameters are given in Table 2. The J01 multiplicity function, originally given as a function of  $\nu$  (Jenkins et al. 2001), is expressed here in terms of  $\nu = \nu_c$ , assuming that  $\nu_c$  is constant although it varies slightly in the  $\Lambda$ CDM universe. In the high-mass range ( $\nu > 1$ ), the numerical multiplicity functions reside between the ST and J01 functions, and its maximum value at  $\nu = 1$  is below those of the ST and J01 functions.

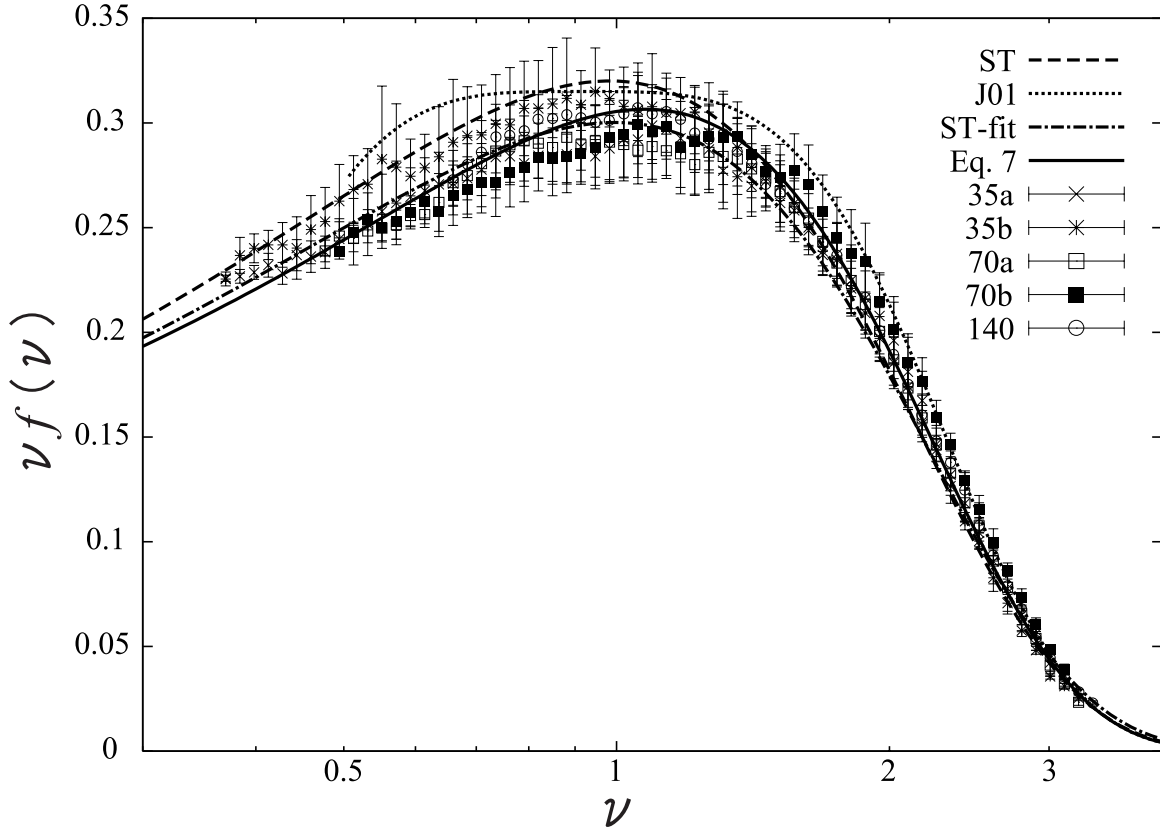


FIG. 3.— The best-fit multiplicity function using equation 7 (solid line). This function well represents the numerical multiplicity functions indicated by symbols with error bars. Also shown for comparison are the ST (dashed line), J01 (dotted line), and best-fit ST (dot-dashed line) functions. For  $1.5 < \nu < 3$ , all the numerical functions reside between the ST and the J01 functions. Even the best-fit ST function cannot represent the multiplicity functions well in this region.

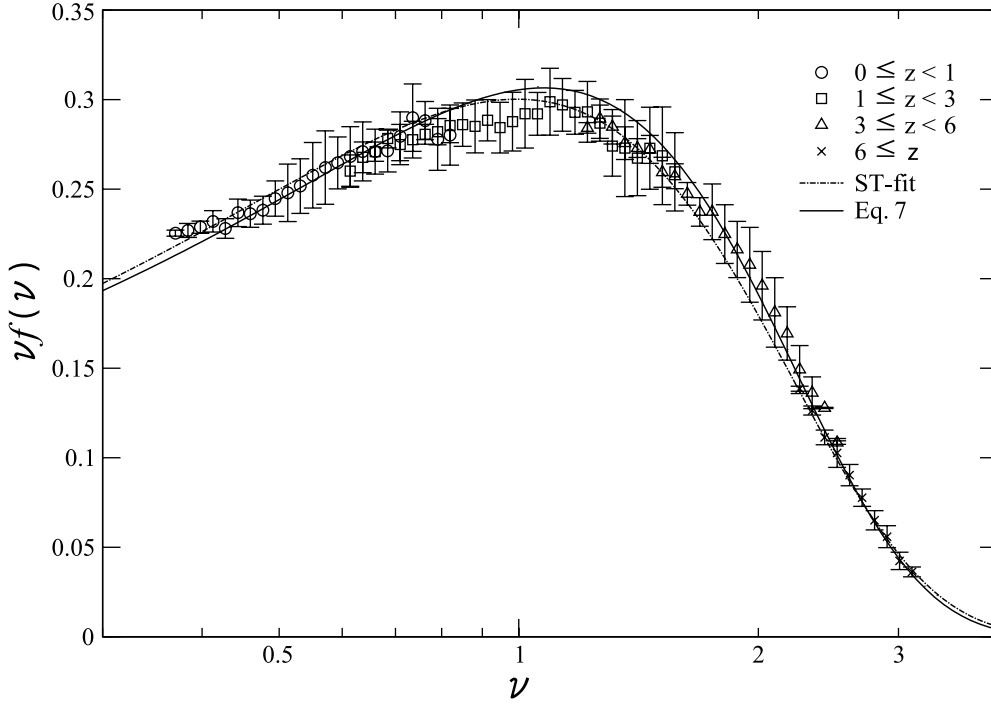


FIG. 4.— Time dependence of the multiplicity function from the 35a run;  $0 \leq z < 1$  (circles),  $1 \leq z < 3$  (squares),  $3 \leq z < 6$  (triangles), and  $z \geq 6$  (crosses). Also shown are the best fit function for all the runs using the ST functional form (dot-dashed line) and equation 7 (solid line). At high redshifts, high- $\nu$  halos in the exponential part of the ST and equation 7 are probed. As redshift decreases, the probe window moves to the lower- $\nu$  region.



TABLE 1. SIMULATION PARAMETERS

Model	$L$ [ $h^{-1}\text{Mpc}$ ]	$m_{\text{ptcl}}$ [ $h^{-1}\text{M}_{\odot}$ ]	$N$	$z_{\text{start}}$
35a ..	35	$2.67 \times 10^7$	$10^7$	50
35b ..	35	$2.67 \times 10^7$	$10^7$	50
70a ..	70	$2.13 \times 10^8$	$10^8$	41
70b ..	70	$2.13 \times 10^8$	$10^8$	41
140 ..	140	$1.70 \times 10^9$	$10^9$	33

NOTE. — All the simulations adopt the cosmological parameters of  $\Omega_m = 0.3$ ,  $\Omega_b = 0.04$ ,  $h = 0.7$ , and  $\Omega_s = 1.0$ . The number of particles is  $512^3$  and the force dynamic range of simulations is  $2^{15} = 32768$  in common.  $L$  is the box size,  $m_{\text{ptcl}}$  is the particle mass, and  $z_{\text{start}}$  is the initial redshift.

TABLE 2. BEST-FIT PARAMETERS

Model	$a$	$p$	$A$	$\max^a$
35a...	0.665	0.317	0.305	0.998
35b...	0.715	0.303	0.320	0.975
70a...	0.666	0.327	0.293	0.988
70b...	0.614	0.325	0.296	1.031
140...	0.658	0.321	0.300	0.999
all...	0.664	0.321	0.301	0.996
PS...	1	0	0.5	1
ST...	0.707	0.3	0.322	0.983
W02.	0.64	0.34	—	0.995

NOTE. — The ST functional form in equation 3 is used to fit to the numerical multiplicity function.

<sup>a</sup>The value of  $\alpha$  at which the best-fit ST function attains a maximum.

TABLE 3. FRACTION OF UNBOUND PARTICLES AT  $z=0$ 

Model	$x_{\text{ub}}^{\text{a}}$
35a ..	0.472
35b ..	0.472
70a ..	0.530
70b ..	0.528
140 ..	0.601

<sup>a</sup>Fraction of unbound particles.